J|A|C|S ARTICLES

Published on Web 06/16/2010

Development and Loss of Ferromagnetism Controlled by the Interplay of Ge Concentration and Mn Vacancies in Structurally Modulated $Y_4Mn_{1-x}Ga_{12-y}Ge_y$

Melanie C. Francisco,[†] Christos D. Malliakas,[†] Paula M. B. Piccoli,[‡] Matthias J. Gutmann,[§] Arthur J. Schultz,[‡] and Mercouri G. Kanatzidis*,[†]

Department of Chemistry, Northwestern University, Evanston, Illinois 60208, Intense Pulsed Neutron Source, Argonne National Laboratory, Argonne, Illinois 60439, and ISIS Facility, Rutherford Appleton Laboratory-STFC, Chilton, Didcot, Oxford OX11 0QX, United Kingdom

Received February 3, 2010; E-mail: m-kanatzidis@northwestern.edu

Abstract: The cubic intermetallic phase $Y_4Mn_{1-x}Ga_{12-y}Ge_y$ ($x = 0-0.26$, $y = 0-4.0$) has been isolated from a molten gallium flux reaction. It presents a rare example of a system where ferromagnetism can be induced by controlling the vacancies of the magnetic centers. The Y_4PdGa_{12} type crystal structure is made up of a corner-sharing octahedral network of Ga and Ge atoms with Mn atoms at the centers of half the octahedra and Y atoms in the voids. At the highest Ge concentration, $y = 4.0$, the Mn site is nearly fully occupied, $x = 0.05$, and the samples are paramagnetic. At a lower Ge concentration, $y = 1.0$, Mn deficiency develops with $x = 0.10$. Surprisingly, strong ferromagnetism is observed with $T_c = 223$ K. When Ge is excluded, $y = 0$, Mn is substantially deficient at $x = 0.26$ and ferromagnetism is maintained with a T_c of $\sim$160 K. In addition, a 6-fold modulated superstructure appears owing to an ordered slab-like segregation of Mn atoms and vacancies. Corresponding bond distortions propagate throughout the octahedral Ga network. Structure−property relationships are examined with X-ray and neutron diffraction, magnetic susceptibility, and electrical resistivity measurements.

1. Introduction

Intermetallic compounds are of interest from both a fundamental and technological point of view. They can exhibit intricate structures[1−4] and a wide range of properties such as superconductivity, ferromagnetism, and heavy fermion behavior,[5−12] but our inability to predict and target specific compositions, structures, and properties underscores significant gaps in our understanding of these materials. To help elucidate new trends and generalize structure−property relationships, we have narrowed our focus on systems composed of rare-earth (RE), transition metal (M), tetrel (Tt), and triel (Tr) elements. The RE and M combination is motivated by the potential interactions of magnetic moments between the two types of spins, localized and itinerant, and the transfer of polarization information between rare earths and transition metals facilitated by the itinerant electrons of the system. This type of mechanism is well described by Ruderman−Kittel−Kasuya−Yosida (*RKKY*) interactions.[13−15]

The RE−M−Tt−Tr compounds can be synthesized through the use of a molten metal flux, which is an excess of a low melting, high boiling point metal used to create a liquid solution of reactants and enhance diffusion rates over traditional solid state synthesis. The triel group (group 13) metals, especially Al through In, are ideal candidates for metal fluxes.[16−25] Tetrel

[†] Northwestern University.
[‡] Argonne National Laboratory.
[§] Rutherford Appleton Laboratory-STFC.

(1) Wu, L.-M.; Seo, D.-K. *J. Am. Chem. Soc.* **2004**, *126*, 4398–4403.
(2) Xia, S.-q.; Bobev, S. *Inorg. Chem.* **2007**, *46*, 874–883.
(3) Mills, A. M.; Mar, A. *Inorg. Chem.* **2000**, *39*, 4599–4607.
(4) Lin, Q.; Corbett, J. D. *Inorg. Chem.* **2007**, *46*, 8722–8727.
(5) Maple, M. B.; Baumbach, R. E.; Hamlin, J. J.; Zocco, D. A.; Taylor, B. J.; Butch, N. P.; Jeffries, J. R.; Weir, S. T.; Sales, B. C.; Mandrus, D.; McGuire, M. A.; Sefat, A. S.; Jin, R.; Vohra, Y. K.; Chu, J. H.; Fisher, I. R. *Phys. B (Amsterdam, Neth.)* **2009**, *404*, 2924–2929.
(6) Miller, G. J. *Chem. Soc. Rev.* **2006**, *35*, 799–813.
(7) Fujii, H.; Okamoto, T.; Shigeoka, T.; Iwata, N. *Solid State Commun.* **1985**, *53*, 715–17.
(8) Coles, B. R. *Contemp. Phys.* **1987**, *28*, 143–157.
(9) Nagamatsu, J.; Nakagawa, N.; Muranaka, T.; Zenitani, Y.; Akimitsu, J. *Nature* **2001**, *410*, 63–64.
(10) Chow, K. H.; MacFarlane, W. A.; Salman, Z.; Fan, I.; Crerar, S. J.; Mar, A.; Egilmez, M.; Jung, J.; Hitti, B.; Arseneau, D. *Phys. B (Amsterdam, Neth.)* **2009**, *404*, 615–618.
(11) Choe, W.; Pecharsky, V. K.; Pecharsky, A. O.; Gschneidner, K. A.; Young, V. G.; Miller, G. J. *Phys. Rev. Lett.* **2000**, *84*, 4617–4620.
(12) Macaluso, R. T.; Nakatsuji, S.; Lee, H.; Fisk, Z.; Moldovan, M.; Young, D. P.; Chan, J. Y. *J. Solid State Chem.* **2003**, *174*, 296–301.
(13) Ruderman, M. A.; Kittel, C. *Phys. Rev.* **1954**, *96*, 99–102.
(14) Kasuya, T. *Prog. Theor. Phys.* **1956**, *16*, 45–57.
(15) Yosida, K. *Phys. Rev.* **1957**, *106*, 893–898.
(16) Zaremba, V. I.; Rodewald, U. C.; Pottgen, R. *Z. Naturforsch., B: Chem. Sci.* **2003**, *58*, 805–808.
(17) Canfield, P. C.; Fisher, I. R. *J. Cryst. Growth* **2001**, *225*, 155–161.
(18) Kanatzidis, M. G.; Pottgen, R.; Jeitschko, W. *Angew. Chem., Int. Ed.* **2005**, *44*, 6996–7023.
(19) Shishido, T.; Tanaka, M.; Horiuchi, H.; Toyota, N.; Fukuda, T. *J. Alloys Compd.* **1992**, *178*, L5–L9.
(20) Latturner, S. E.; Bilc, D.; Mahanti, S. D.; Kanatzidis, M. G. *Chem. Mater.* **2002**, *14*, 1695–1705.
(21) Fehrmann, B.; Jeitschko, W. *Inorg. Chem.* **1999**, *38*, 3344–3351.
(22) Xia, S.-q.; Hullmann, J.; Bobev, S.; Ozbay, A.; Nowak, E. R.; Fritsch, V. *J. Solid State Chem.* **2007**, *180*, 2088–2094.
(23) Lei, X.-W.; Zhong, G.-H.; Li, L.-H.; Hu, C.-L.; Li, M.-J.; Mao, J.-G. *Inorg. Chem.* **2009**, *48*, 2526–2533.
(24) Chondroudi, M.; Balasubramanian, M.; Welp, U.; Kwok, W.-K.; Kanatzidis, M. G. *Chem. Mater.* **2007**, *19*, 4769–4775.

 10.1021/ja1009986

elements (group 14) are added to the reaction to provide refractory properties and can also add further functionality and complexity to the electronic structure.

A rational starting point for investigations is with the transition metals Fe, Ni, and Co as they are ferromagnetic in their elemental state. Many compounds of the RE−M−Tr type have been synthesized, where M = Fe, Ni, or Co, with often the same outcome that the transition metal is reduced and its magnetic moment quenched consequently becoming diamagnetic.[24,26−30] Density functional theory calculations on these types of compounds have shown that the transition metal 3*d* band lies well below the Fermi level and is filled (i.e., $3d^{10}$) and diamagnetic.[31−34] In addition, for *p*-metal rich compounds, the extensive interaction between the *d*-orbitals of transition metals and *p*-orbitals of trielides and tetrelides works to increase the separation between bonding and antibonding energy bands and deplete electron density at the Fermi level.[35,36] Thus, with a low density of states at the Fermi level, it is difficult to satisfy the criterion for spontaneous magnetization given by the Stoner condition, $I \times DOS(E_F) > 1$, where *I* is the Stoner parameter.[37] These trends led us to move toward the more electropositive element Mn where we expected higher resistance of the *d*-orbitals to being filled in these compounds and thus retention of a magnetic moment originating from Mn.

Exploration in the Y−Mn−Ga−Ge system, with Ga being the metallic flux, led to the new compounds $Y_4Mn_{1-x}Ga_{12-y}Ge_y$, isotypic with the quaternary family $RE_4FeGa_{12-x}Ge_x$ (RE = Tb, Sm, Y).[38] The compounds crystallize in the Y_4PdGa_{12} structure type,[39−45] a variant of the $U_4Re_7Si_6$ structure,[46] in the $Im\bar{3}m$ space group. $Tb_4FeGa_{12-x}Ge_x$ was reported to order antiferromagnetically with an effective moment close to the theoretical value for the free RE ion. Mössbauer spectroscopy measurements confirmed that the iron is in a reduced, diamagnetic state.[38] On the other hand, we find that $Y_4Mn_{1-x}Ga_{12-y}Ge_y$ orders ferromagnetically at a high Curie temperature with high susceptibility and observe a strong correlation between the parameter *y* and the magnetism of this system. To clarify this correlation, we studied a series of compounds for $y = 0-4$ and found an inverse relationship between Ge concentration and magnetic properties. Samples of low Ge content showed higher transition temperatures than those of higher Ge content. Single crystal X-ray structure refinements for the quaternary compounds were complicated by the low contrast in scattering strengths between Ga and Ge (∼3%). To decipher the Ga from the Ge site, neutron diffraction data were also collected. The diffraction experiments were supplemented by elemental analysis using energy dispersive spectroscopy and atomic emission spectroscopy. In the Ge-free ternary compound $Y_4Mn_{1-x}Ga_{12}$ ($y = 0$) we observed additional satellite peaks in the single crystal X-ray diffraction pattern revealing a 6-fold structural modulation. The supercell structure was solved with superspace crystallographic methods[47−50] and showed long-range ordering of Mn vacancies and consequent distortions of bond lengths. The presence of Mn magnetic centers in this structure type creates a unique combination of properties including ordered vacancies, positional modulations, and spontaneous magnetization that are controlled by the interplay of Ge atom concentration and Mn vacancies.

2. Experimental Section

2.1. Reagents. Yttrium powder (Sigma-Aldrich, 99.9% (REO)) and manganese powder (Sigma-Aldrich, 99.99%) were used as obtained from the manufacturer. Ge shavings (Plasmaterials, 99.9999%) were ground, and Ga tear drops (Plasmaterials, 99.999%) were crushed after freezing in liquid nitrogen.

2.2. Synthesis. Yttrium (0.133 g, 1.5 mmol), manganese (0.041 g, 0.75 mmol), germanium (0.0277 g, 0.375 mmol), and excess gallium (1.5709 g, 22.5 mmol) were combined in an alumina crucible and inserted into fused silica tubes in a nitrogen-filled glovebox. A small amount of ceramic fiber was added to cover the opening of the crucible for high-temperature centrifugation posttreaction. The fused silica tubes were flame-sealed under vacuum ($<10^{-3}$ mbar). The samples were heated to 1000 °C (59 °C/h) and soaked for 5 h, cooled to 850 °C (75 °C/h), isothermally heated for 36 h, and then cooled to 250 °C (12 °C/h). The tubes were inverted and centrifuged while hot for ∼30 s at high speed (∼3000

(25) Okudzeto, E. K.; Kuga, K.; Nakatsuji, S.; Chan, J. Y. *Cryst. Growth Des.* **2009**, *9*, 1956–1959.
(26) Zhuravleva, M. A.; Kanatzidis, M. G. *Inorg. Chem.* **2008**, *47*, 9471–9477.
(27) Latturner, S. E.; Kanatzidis, M. G. *Inorg. Chem.* **2008**, *47*, 2089–2097.
(28) Anand, V. K.; Hossain, Z.; Geibel, C. *Solid State Commun.* **2008**, *146*, 335–339.
(29) Baran, S.; Gondek, L.; Hernandez-Velasco, J.; Kaczorowski, D.; Szytula, A. *J. Magn. Magn. Mater.* **2006**, *305*, 196–201.
(30) Cho, J. Y.; Millican, J. N.; Capan, C.; Sokolov, D. A.; Moldovan, M.; Karki, A. B.; Young, D. P.; Aronson, M. C.; Chan, J. Y. *Chem. Mater.* **2008**, *20*, 6116–6123.
(31) Gout, D.; Benbow, E.; Gourdon, O.; Miller, G. J. *J. Solid State Chem.* **2003**, *174*, 471–481.
(32) Matar, S. F.; Riecken, J. F.; Chevalier, B.; Pottgen, R.; Al Alam, A. F.; Eyert, V. *Phys. Rev. B: Condens. Matter* **2007**, *76*, 174434/1–174434/6.
(33) Salvador, J. R.; Hoang, K.; Mahanti, S. D.; Kanatzidis, M. G. *Inorg. Chem.* **2007**, *46*, 6933–6941.
(34) Wu, X.; Francisco, M.; Rak, Z.; Bakas, T.; Mahanti, S. D.; Kanatzidis, M. G. *J. Solid State Chem.* **2008**, *181*, 3269–3277.
(35) Kim, S.-H.; Bostroem, M.; Seo, D.-K. *J. Am. Chem. Soc.* **2008**, *130*, 1384–1391.
(36) Landrum, G. A.; Dronskowski, R. *Angew. Chem., Int. Ed.* **2000**, *39*, 1560–1585.
(37) Stoner, E. C. *Philos. Mag.* **1933**, *15*, 1018–34.
(38) (a) Zhuravleva, M. A.; Wang, X.; Schultz, A. J.; Bakas, T.; Kanatzidis, M. G. *Inorg. Chem.* **2002**, *41*, 6056–6061. (b) Salvador, J. R.; Bilc, D.; Mahanti, S. D.; Kanatzidis, M. G. *Angew. Chem. Int. Ed.* **2003**, *42*, 1929–1932. (c) Zhuravleva, M. A.; Pcionek, R. J.; Wang, X. P.; Schultz, A. J.; Kanatzidis, M. G. *Inorg. Chem.* **2003**, *42*, 6412–6424. (d) Sieve, B.; Chen, X. Z.; Henning, R.; Brazis, P.; Kannewurf, C. R.; Cowen, J. A.; Schultz, A. J.; Kanatzidis, M. G. *J. Am. Chem. Soc.* **2001**, *123*, 7040–7047. (e) Zhuravleva, M. A.; Chen, X. Z.; Wang, X. P.; Schultz, A. J.; Ireland, J.; Kannewurf, C. K.; Kanatzidis, M. G. *Chem. Mater.* **2002**, *14*, 3066–3081. (f) Salvador, J. R.; Gu, F.; Hogan, T.; Kanatzidis, M. G. *Nature* **2003**, *425*, 702–705.
(39) Vasilenko, L. O.; Noga, A. S.; Grin, Y. N.; Koterlin, M. D.; Yarmolyuk, Y. P. *Izvestiya Akademii Nauk SSSR. Metally* **1988**, *5*, 216–220.
(40) Gumeniuk, R.; Stel'makhovych, B. M.; Kuz'ma, Y. B. *J. Alloys Compd.* **2003**, *352*, 128–133.
(41) Jardin, R.; Colineau, E.; Wastin, F.; Rebizant, J.; Sanchez, J. P. In *International Conference on Strongly Correlated Electron Systems (SECES 05)*; Vienna, Austria, 2005; pp 1031−1032.
(42) Williams, W. M.; Moldovan, M.; Young, D. P.; Chan, J. Y. *J. Solid State Chem.* **2005**, *178*, 52–57.
(43) Jardin, R.; Colineau, E.; Wastin, F.; Rebizant, J.; Sanchez, J. P. *Phys. B (Amsterdam, Neth.)* **2006**, *378−380*, 1031–1032.
(44) Jardin, R.; Colineau, E.; Griveau, J. C.; Boulet, P.; Wastin, F.; Rebizant, J. *J. Alloys Compd.* **2007**, *432*, 39–44.
(45) Drake, B. L.; Grandjean, F.; Kangas, M. J.; Okudzeto, E. K.; Karki, A. B.; Sougrati, M. T.; Young, D. P.; Long, G. J.; Chan, J. Y. *Inorg. Chem.* **2010**, *49*, 445–456.
(46) Aksel'rud, L. G.; Yarmolyuk, Y. P.; Gladyshevskii, E. I. *Dopovidi Akademii Nauk Ukrains'koi RSR, Seriya A: Fiziko-Matematichni ta Tekhnichni Nauki* **1978**, *4*, 359–62.
(47) de Wolff, P. M. *Acta Crystallogr., Sect. A* **1974**, *30*, 777–785.
(48) de Wolff, P. M.; Janssen, T.; Janner, A. *Acta Crystallogr., Sect. A* **1981**, *37*, 625–636.
(49) Petricek, V.; Dusek, M. *Zeitschrift Fur Kristallographie* **2004**, *219*, 692–700.
(50) van Smaalen, S. *Z. Kristallogr.* **2004**, *219*, 681–691.

rpm) to remove unreacted Ga flux. The remaining product was soaked overnight in 3 M I_2 in *N*,*N*-dimethylformamide (DMF) solution to remove residual gallium and then washed with DMF, hot water, and acetone over vacuum filtration. Typical crystal dimensions are roughly 0.3 mm and up to 1.5 mm. Yield was approximately 20% based on starting rare earth amount and 60% by mass of the solid product. Bulk PXRDs of the reaction batches before etch treatment indicated the presence of $MnGa_4$, $Y(Ga,Ge)_6$, $Y(Ga,Ge)_2$, and the unreacted elements, in addition to the cubic 4−1−12 phase. Single crystals used for characterization were hand-picked and confirmed to be the correct phase by energy dispersive spectroscopy. To facilitate selection, magnetic crystals could be cooled in a liquid nitrogen bath and separated from other phases with a magnet. Sensitivity to air or moisture was not observed.

Alternatively to the above method, the ternary phase can also be synthesized following the published heating profile for Tb_4PdGa_{12}.[42] Yttrium (0.068 g, 1 mmol), manganese (0.041 g, 1 mmol), and excess gallium (1.0532 g, 20 mmol) were combined in an alumina crucible and sealed in the same manner as mentioned above. The tube was heated to 1150 °C over 7 h, slowly cooled to 530 °C over 41 h, then cooled down to 300 °C in 2 h, inverted, and centrifuged to remove excess Ga flux.

2.3. Characterization Methods. 2.3.1. Single-Crystal X-ray Diffraction. Single-crystal X-ray diffraction data were collected at 100 K on a STOE 2T image plate diffractometer with Mo Kα radiation (λ = 0.710 73 Å) using the X-Area suite of programs provided by STOE.[51] Data were collected on several single crystals, each covering a full sphere of reciprocal space. An analytical absorption correction was applied using the program X-Red on an optimized shape obtained with the aid of X-Shape software. The structures were solved with direct methods and refined with the SHELXTL software package.[52] Thermal displacement parameters were anisotropically refined for all atomic positions.

Satellite reflections of the first order were observed and used for the refinement of the ternary $Y_4Mn_{1-x}Ge_{12}$ compound using the Jana2006 refinement program.[53] A single modulation wave for positional and thermal (Y and Ga only) parameters was used for all the atoms. Additionally, an occupational orthogonal step-like function, the Crenel function,[54] was used to describe the discontinuous modulation of the Mn atoms due to a long-range ordering of vacancies. Only the symmetry allowed Fourier terms above the standard uncertainty were refined.

2.3.2. Single-Crystal Neutron Diffraction: Paramagnetic Sample. Neutron diffraction data were obtained at the Intense Pulsed Neutron Source (IPNS) at Argonne National Laboratory using the time-of-flight Laue single-crystal diffractometer (SCD).[55] A crystal with approximate dimensions of 1.5 × 1.5 × 1.5 mm^3 and a weight of 16.0 mg was wrapped in aluminum foil and glued to an aluminum pin that was mounted on the cold stage of a closed-cycle helium refrigerator. The crystal was maintained under vacuum at a temperature of 298 ± 1 K. An autoindexing algorithm[56] was used to obtain an initial orientation matrix from the peaks in three preliminary histograms measured for 30 min each. For intensity data collection, runs of 2 h per histogram were initiated for the data set. Settings were arranged at χ and φ values suitable to cover at least one unique octant of reciprocal space (Laue symmetry $m\bar{3}m$). With the above counting times, 10 histograms were completed in the 6 days available for the experiment. Bragg peaks in the recorded histograms were indexed and integrated using individual orientation matrices for each histogram to allow for any misalignment of the sample. Intensities were integrated about their predicted locations and were corrected for the Lorentz factor, the incident spectrum, and the detector efficiency. A wavelength-dependent spherical absorption correction was applied using cross sections from Sears[57] (μ (cm^{-1}) = 0.387 + 0.086λ). Symmetry-related reflections were not averaged since different extinction factors are applicable to reflections measured at different wavelengths.

2.3.3. Ferromagnetic Sample. Neutron single crystal diffraction data were collected at 260 K, above the sample Curie temperature, using the time-of-flight Laue diffractometer SXD installed at the ISIS pulsed neutron source (Oxfordshire, U.K.).[58] The 1.3 × 1.3 × 1.3 mm^3, 8.0 mg crystal was mounted at the end of an Al pin using a strip of adhesive Al tape inside a closed-cycle He refrigerator. Five exposures in different crystal orientations were taken for 1 h each. Data were processed using the locally available SXD2001 software.[59]

2.3.4. Powder X-ray Diffraction (PXRD). Purity was checked by PXRD on an Inel CPS120 in reflectance mode using Cu Kα radiation (λ = 1.5406 Å). Single crystals were ground and applied to double-sided tape attached to a borosilicate microscope slide. Data was collected for 2 h (see Supporting Information). Weak impurity peaks could be indexed to elemental β-Mn and γ-Ga, most likely remaining in microcracks in the crystal.

2.3.5. Energy Dispersive Spectroscopy Analysis (EDS). Approximate elemental compositions were obtained by quantitative microprobe analysis performed on a Hitachi S3400-N VP-Secondary Electron Microscope (SEM) equipped with an Oxford Instruments INCA detector. Detector operating parameters were optimized prior to data analysis by collecting a Cu spectrum. Data were collected on single crystals fixed on carbon tape with an accelerating voltage of 25 kV and 45−60 s accumulation times. Samples were not polished, and many data points were collected to evaluate error. Deviations in homogeneity within a crystal were less than 10%. Relative deviations for crystals both within a synthetic batch of crystals and between batches of identical reactions were approximately or less than 15%.

2.3.6. Inductively Coupled Plasma-Atomic Emission Spectroscopy (ICP-AES). Elemental compositions of single crystals were measured on a Varian Vista-MPX Inductively Coupled Plasma Optic Emission Spectrometer system. Clean single crystals were dissolved in acid solution, and the solutions were diluted with deionized water. The etchant solution consisted of 35 mL of HNO_3 (dil. 1:1), 5 mL of HCl (dil. 1:1), and 1 g of tartaric acid. This ratio has been shown to minimize loss of germanium due to volatization of chloride complexes.[60] Standards were prepared from 1000 ± 1 ppm stock solutions (GFS Chemicals) in the appropriate concentration range. Wavelengths were selected as follows: Y, 371.029 nm; Mn, 257.610 nm; Ga, 417.204 nm; Ge, 209.426 nm. Calibration correlation coefficients were greater than 99.999%.

2.3.7. Magnetic Susceptibility. DC magnetic susceptibility measurements were performed on a computer-controlled Quantum Design SQUID Magnetometer (MPMS5). Single crystals (∼2 mg) were mounted on Kapton tape. Field dependent measurements were first collected at 5 and 300 K between ±5 T. Zero-field (ZF) and field-cooled (FC) (10 K/min) temperature dependent studies were collected at 0.08 T, within the linear region of the 5 K hysteresis loops, from 1.8 to 300 K. Data were corrected for the core diamagnetic contribution calculated from Pascal's constants.

(51) STOE & Cie GmbH. *X-AREA*, V.; STOE & Cie GmbH: Darmstadt, Germany, 2006.
(52) Sheldrick, G. M. S. S. D. P. *SHELXTL*, version 6.14, 2000−2003. Bruker AXS Inc., Madison, WI.
(53) Petricek, V. D., M. g; Palatinus, L. *Jana2006. The crystallographic computing system*; Institute of Physics: Praha, Czech Republic, 2006.
(54) Petricek, V.; van der Lee, A.; Evain, M. *Acta Crystallogr., Sect. A* **1995**, *A51*, 529–35.
(55) Schultz, A. J.; De Lurgio, P. M.; Hammonds, J. P.; Mikkelson, D. J.; Mikkelson, R. L.; Miller, M. E.; Naday, I.; Peterson, P. F.; Porter, R. R.; Worlton, T. G. *Phys. B (Amsterdam, Neth.)* **2006**, *385−386*, 1059–1061.
(56) Jacobson, R. A. *J. Appl. Crystallogr.* **1976**, *19*, 283–286.
(57) Sears, V. F. *Methods of Experimental Physics, Vol. 23, Neutron Scattering, Part A*; Academic Press: Orlando, FL, 1986.
(58) Keen, D. A.; Gutmann, M. J.; Wilson, C. C. *J. Appl. Crystallogr.* **2006**, *39*, 714–722.
(59) Gutmann, M. *Acta Crystallogr., Sect. A* **2005**, *61*, c164.
(60) Shoji, T.; Danzaki, Y.; Ashino, T.; Konno, H.; Makabe, K.-i. *Bunseki Kagaku* **2000**, *49*, 709–712.

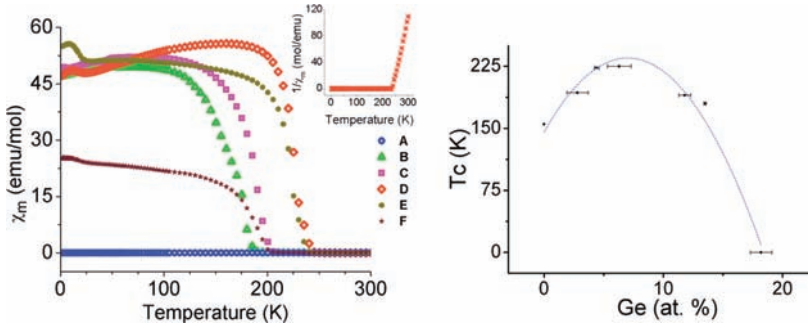

Figure 1. (Left) Magnetic susceptibility of a series of $Y_4Mn_{1-x}Ga_{12-y}Ge_y$ samples measured in an applied field of 80 G. Ge content decreases from A to F. T_c increases from A to D/E and decreases to F. The inset graph shows the linear inverse susceptibility of sample D above the transition temperature. Compositional analyses for samples A−F are given in Table 1. (Right) Curie temperature are plotted against average at. % Ge determined by EDS. One standard deviation error bars for Ge are drawn.

Table 1. Starting Molar Ratios and Elemental Compositions for the Series of Samples of $Y_4Mn_{1-x}Ga_{12-y}Ge_y$ Shown in Figure 1[a]

	Rxn ratios Y/Mn/Ge/Ga	Composition (EDS)	Composition (ICP-AES)	T_c (K)	C (mol/emu)	Θ (K)	μ_{eff} (μ_B/mol)
A	4:2:4:60	$Y_{4.3(3)}Mn_{0.88(3)}Ga_{8.8(4)}Ge_{3.1(2)}$	$Y_{4.14(3)}Mn_{0.91(9)}Ga_{9.02(6)}Ge_{2.83(4)}$	−	n/a	n/a	
B	4:1:2:60	$Y_{4.3(4)}Mn_{0.85(3)}Ga_{9.4(7)}Ge_{2.3(3)}$		180	1.02(3)	170(10)	2.85(4)
C	6:1:2:60	$Y_{4.5(2)}Mn_{0.82(1)}Ga_{8.2(1)}Ge_{2.0(1)}$		190	0.37(3)	210(30)	1.73(6)
D	4:2:1:60	$Y_{4.2(4)}Mn_{0.89(3)}Ga_{10.7(5)}Ge_{1.1(2)}$		225	0.76(2)	240(10)	2.47(3)
E	4:2:0.65:60	$Y_{4.1(2)}Mn_{0.87(2)}Ga_{10.6(2)}Ge_{1.2(7)}$	$Y_{4.11(3)}Mn_{0.89(1)}Ga_{11.(8)}Ge_{0.81(1)}$	223	0.568(8)	238(8)	2.13(2)
F	4:2:0.5:60	$Y_{4.6(2)}Mn_{0.86(3)}Ga_{10.9(2)}Ge_{0.5(1)}$		193	n/a	n/a	

[a] Magnetic parameters for high temperature data that follow a Curie−Weiss model are also given.

2.3.8. Electrical Resistivity. Copper contacts were attached to single crystals using colloidal silver paste in a linear four-probe configuration. Temperature-dependent resistivity measurements were taken on a Quantum Design Physical Properties Measurement System (PPMS) from 1.8 to 300 K.

3. Results and Discussion

The compounds with formula $Y_4Mn_{1-x}Ga_{12-y}Ge_y$ crystallize in the cubic space group $Im\bar{3}m$ in the Y_4PdGa_{12} structure type.[38−40,43,44] They can be synthesized from different starting ratios and showed variable magnetic behavior with both ferromagnetic and paramagnetic phases formed depending on composition. Crystals of $Y_4Mn_{1-x}Ga_{12-y}Ge_y$ were first isolated from one of a series of reactions of differing starting ratios in the Y−Mn−Ga−Ge system. Initial magnetic measurements on a sample of single crystals showed ferromagnetic ordering at a T_c of ∼100 K. Since this original synthesis produced a low yield of single crystals, other starting ratios and reaction conditions were used to improve the synthesis. Magnetic susceptibility measurements on a sample from a higher yield reaction (Y:Mn:Ge:Ga = 2:1:2:30) unexpectedly showed no magnetic ordering. Surprisingly, another sample (Y:Mn:Ge:Ga = 2:1:1:30) then showed a ferromagnetic response with a T_c of ∼200 K. Compositional analysis on a series of samples from different syntheses revealed the subtle differences in Ge concentration in each sample suggesting the magnetic properties to be strongly dependent on the Ga/Ge ratio. We first present the magnetic properties as a function of composition and then analyze the crystal structure to determine structure−property relationships. The modulated X-ray structure solution of the ternary compound $Y_4Mn_{1-x}Ga_{12}$, which contains additional ordering of Mn atoms and vacancies, is also discussed.

3.1. Magnetic Properties and Composition. Temperature-dependent magnetic susceptibility measurements on single crystals, as well as compositions determined by EDS and ICP-AES, are shown in Figure 1 and Table 1. The relationship between molar starting ratios and resulting crystal composition

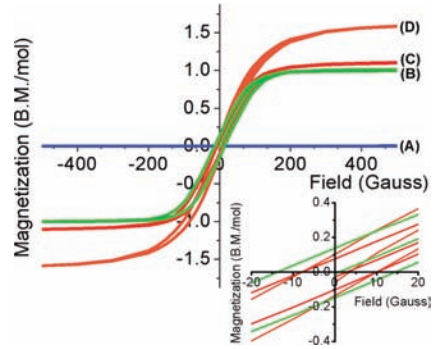

Figure 2. Magnetic hysteresis loops taken at 5 K. Inset shows an enlarged region about the origin to show coercivity of the soft magnets. Sample compositions A−D are given in Table 1.

is not directly 1:1 owing to the nature of the flux method and variations in solution equilibrium between phases (e.g., $MnGa_4$, $Y(Ga,Ge)_6$, etc.) as ratios are varied. Germanium can be relatively varied, however, by a corresponding increase or decrease in starting Ge molar concentration. Samples B and C imply, with a constant Ga:Ge starting molar ratio, that the amount of Ge incorporated in the final product is not largely affected by changes in Y starting molar concentration.

Magnetic hysteresis loops shown in Figure 2 were collected at 5 K and indicate soft magnetic properties with a coercive field of less than 20 G and remnant magnetization less than 0.2 μ_B/mol. The Curie−Weiss model ($\chi = C/(T - \theta)$) was used to extract magnetic parameters from the linear inverse susceptibility data in the paramagnetic region. Data above T_c was not linear for samples A and F; attempts to fit to a Curie−Weiss law with a temperature-independent parameter ($\chi = [C/(T - \theta)] + \chi_o$) did not give reasonable parameters and are not reported in Table 1.

The samples order ferromagnetically, as determined by the large and positive Weiss temperatures, with Curie temperatures that relate to Ge concentration. The absolute composition of single crystals is difficult to discern considering the small

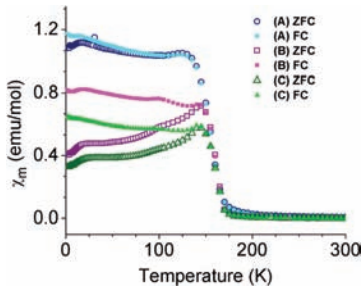

Figure 3. Zero-field and field-cooled temperature dependent magnetic susceptibilities of the parent ternary phase $Y_4Mn_{1-x}Ga_{12}$ grown from different batches of starting ratios: (A) 1Y:1Mn:20Ga [alternative synthesis] at 500 G; (B) 2Y:1/2Mn:30Ga at 80 G; (C) 1Y:2Mn:30Ga at 100 G.

amount of Mn and Ge relative to Ga and Y; the EDS spectrum is dominated by the elements of greater concentration. To gain the most confident values, multiple crystals and points of analysis on samples from the same and different batches were collected and averaged. Figure 1 (right) shows the relationship between the Curie temperature, T_c, versus at % Ge with one standard deviation error bars. At the largest fraction of Ge, the samples are paramagnetic. As Ge concentration decreases, T_c increases to a maximum of nearly 230 K (Y:Mn:Ge:Ga = 4:2:1:60) and then eventually decreases with lower Ge content (Y:Mn:Ge:Ga = 4:2:0.4:60). As will be discussed, atomic positional distortions as well as Mn vacancies begin to develop as Ge decreases from the paramagnetic phase. This increase in local disorder may explain the turnover in T_c after less than ~8 at % Ge, or $y = 1$.

A clear trend in the relative concentration of Mn in each sample was not observed by means of EDS and ICP-AES. We attempted to extract Mn occupancy through multiple single-crystal XRD collections and refinement of the site occupancy factor on the single Mn position. Again there was no clear trend between Mn concentration and T_c or Ge. The extreme comparison between quaternary samples (>95% Mn site occupancy by XRD) and the parent ternary compound, $y = 0$ (74% Mn occupancy), does clearly show that the absence of Ge causes a significant Mn deficiency. We rely on neutron diffraction, a much more sensitive probe for site occupancy, to determine variation in Mn occupation between different quaternary samples.

The Ge-free ternary compound $Y_4Mn_{1-x}Ga_{12}$ also shows ferromagnetic ordering, although with much lower susceptibility and at a lower T_c. The increase in Mn vacancies in comparison to the quaternary phases could explain the large decrease in intensity. Magnetic susceptibility plots of $Y_4Mn_{1-x}Ga_{12}$ crystals from three different preparations, and under different applied fields, are graphed in Figure 3. The three ternary samples analyzed have a relatively sharp transition temperature, ~155 K. As the susceptibility plots show, T_c is invariant to changes in reaction starting ratios and the synthetic route for the ternary parent compound $Y_4Mn_{0.74}Ga_{12}$.

A significant difference between zero-field cooled (ZFC) and field-cooled (FC) plots exists, which is not observed in the quaternary ferromagnetic phase. The divergence, or bifurcation, is nearly eliminated under the higher applied field of 500 G for sample A. This suggests magnetic domains become pinned on cooling until alignment occurs under an applied field and increase in temperature. It is unclear why this hysteresis develops in the ternary phase and not the quaternary phase; however, as will be discussed, crystallographic segregation of the Mn atoms and positional modulation occurs in the ternary phase, and this may lead to the development of more stable pinned states.

The effective moment of Mn (~2 μ_B) in $Y_4Mn_{1-x}Ga_{12-y}Ge_y$, assuming diamagnetic Y^{3+}, is slightly lower than that of elemental Mn[61] (2.4 μ_B) and significantly lower than simple Mn-containing intermetallic compounds (e.g., 4.12 μ_B in Cu_2MnAl[62] and 5.0 μ_B in $MnTe_2$[63,64]). The saturated moment of ~1.5 μ_B/Mn is comparable to that of Mn_2Ga_5, with 1.36 μ_B/Mn.[35] The presence of a magnetic moment suggests that the Fermi level lies within orbitals with a strong Mn contribution and the *d*-orbital bands in these compounds are not completely filled, in contrast to many Fe-, Ni-, and Co-containing intermetallics. For *p*-metal rich intermetallic phases, this relatively rare group of compounds in which the transition metal retains a magnetic moment include the previously mentioned Mn_2Ga_5[35] and also $RECrGe_3$.[65]

3.2. Resistivity. The temperature dependent resistivity data for a single crystal of ferromagnetic $Y_4Mn_{1-x}Ga_{12-y}Ge_y$ ($1.0 < y < 4.0$) is shown in Figure 4. The resistivity value at 250 K, ca. 1.0 mΩ·cm, and linear increase with temperature are consistent with metallic behavior. The magnetic transition temperature is reflected as a small change in the resistivity slope, indicated in the figure. A zoomed region around the transition is provided in Figure 4 as well as an overlay plot of the derivative to show the difference in slope. The crystal was made from starting molar ratios 4Y:2Mn:2Ge:60Ga. A magnetic transition slightly below 200 K would be expected by comparison to Figure 1 and Table 1 (similar to Samples B and C). In addition, an anomalous drop in resistivity is observed below ~7 K. An applied field of 1000 G eliminates the drop in resistivity at low temperature and is possibly the superconducting transition of elemental λ-gallium (7.62 K)[66] that remains in microcracks after etching.

3.3. Crystal Structure. 3.3.1. Quaternary Compounds $Y_4Mn_{1-x}Ga_{12-y}Ge_y$. Single crystal X-ray diffraction studies

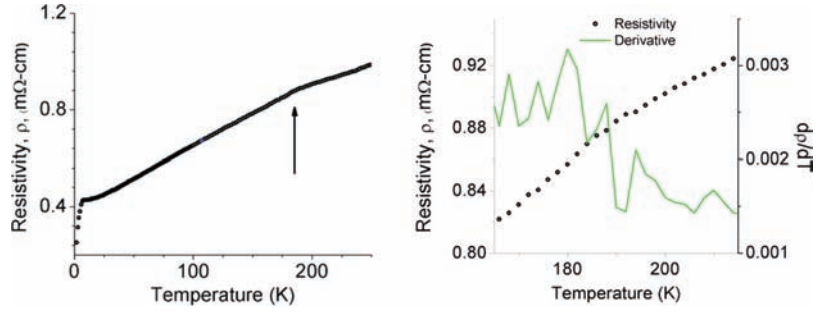

Figure 4. (Left) Temperature-dependent resistivity of a ferromagnetic sample of $Y_4Mn_{1-x}Ga_{12-y}Ge_y$. The arrow indicates the change in slope associated with the magnetic transition. (Right) A zoomed region of the magnetic transition plotted against the slope of resistivity versus temperature.

Table 2. Atomic Coordinates for Paramagnetic (p) and Ferromagnetic (f) $Y_4Mn_{1-x}Ga_{12-y}Ge_y$ from Neutron Refinements

		x				Site occupancy		U_{eq} ($\times 10^{-3}$ Å^2)[a]	
	Wyckoff Site	(p)	(f)	*y*	*z*	(p)	(f)	(p)	(f)
Y1	8*c*	0.25		0.25	0.25	1		6.1(3)	6.9(3)
Mn1	2*a*	0		0	0	0.95(2)	0.90(3)	9(1)	10(2)
Ga1/Ge1	12*d*	0.25		0	0.5	0.66(5)/0.34(5)	1/0	6.1(4)	10.9(4)
Ga2/Ge2	12*e*	0.2892(2)	0.2895(2)	0	0	0.67(5)/0.33(5)	0.83(6)/0.17(6)	8.1(3)	10.9(4)

[a] U_{eq} is defined as one-third of the trace of the orthogonalized U_{ij} tensor.

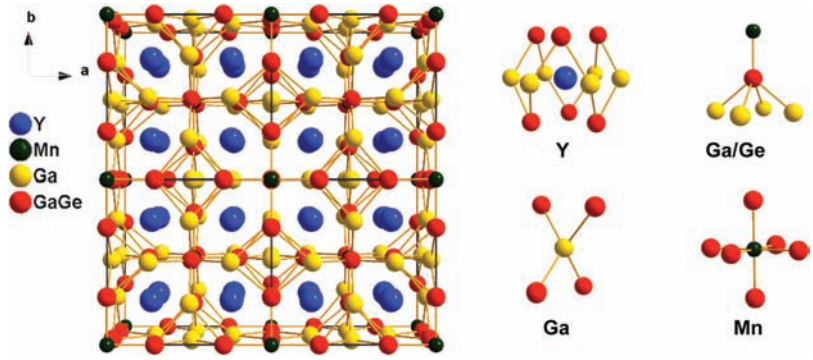

Figure 5. Crystal structure of $Y_4Mn_{0.95}Ga_{11.0}Ge_{1.0}$ from neutron diffraction refinement. (Left) 2 × 2 × 2 expanded cell viewed down the *c*-axis. (Right) Local environments of Y, Ga1 (Ga1/Ge1 for the paramagnetic sample), Ga2/Ge2, and Mn.

confirmed that the compounds adopt the $Im\bar{3}m$ space group with cell parameters in the range $a = 8.54-8.6$ Å. Using an arbitrary Ga/Ge assignment, the largest residual electron density was found just off the Ge site in the ferromagnetic phase and was consistently present in the X-ray refinements of the several ferromagnetic crystals screened. This was not observed in the case of the paramagnetic species. Neutron diffraction was used to resolve Ga and Ge disorder in the crystal structure. Atomic coordinates from the X-ray collections were used as a starting point for refinements. Refined coordinates are given in Table 2.

The atoms arrange on four unique crystallographic positions at Wyckoff sites 2*a*, 8*c*, 12*d*, and 12*e* as shown in Figure 5. The Y and Mn atoms occupy sites 8*c* and 2*a*, respectively. Ga and Ge are distributed between the 12*d* and 12*e* sites in the crystal.

Several disordered structural models were tested to determine the distribution of Ga and Ge over the 12*d* and 12*e* sites. The final refinement was based on the goodness of fit parameter and comparison to ICP-AES results performed on single crystals synthesized under the same reaction conditions as those for the single crystals used in the diffraction experiment. For the paramagnetic sample, the best model was a mixed Ga and Ge occupancy on both 12*d* and 12*e* sites. For the ferromagnetic sample, only the 12*e* site could be disordered while still being in reasonable agreement with elemental analyses. The site occupancy at the Mn site was refined and found to be slightly deficient, more so for the ferromagnetic sample. The occupancy factor of Y on the 8*c* site was also refined and found to be fully occupied in both samples. Refined occupancies are given in Table 2. The final compositions for the paramagnetic and ferromagnetic crystal are $Y_4Mn_{0.95(2)}Ga_{8.0(6)}Ge_{4.0(6)}$ and $Y_4Mn_{0.90(3)}Ga_{11.0(4)}Ge_{1.0(4)}$, respectively. Crystallographic data for both paramagnetic and ferromagnetic single crystals are presented in Table 3. Select bond lengths are given in Table 4.

Table 3. Crystal Data from Neutron Diffraction and Structure Refinement Parameters for the Joint X-ray and Neutron Refinement

Formula	$Y_4Mn_{0.95(2)}$ $Ga_{8.0(6)}Ge_{4.0(6)}$	$Y_4Mn_{0.90(3)}Ga_{11.0(4)}Ge_{1.0(4)}$
Rxn starting molar ratios	4Y:2Mn:4Ge:60Ga	4Y:2Mn:0.65Ge:60Ga
Magnetic properties	Paramagnetic	Ferromagnetic
fw	1255.96	1244.88
Temperature, K	298(1)	260(1)
Crystal system	*cubic*	*cubic*
Space group	$Im\bar{3}m$	$Im\bar{3}\bar{m}$
a, Å	8.586(2)	8.5980(27)
V, Å^3	633.0(3)	635.61(35)
Z	2	2
d_{calc}, g cm^{-3}	6.588	6.504
Size, mm^3	1.5 × 1.5 × 1.5	1.3 × 1.3 × 1.3
Radiation	neutrons	neutrons
Data collection technique	time-of-flight Laue	time-of-flight Laue
$\mu(\lambda)$, cm^{-1}	0.387 + 0.154 λ	0.367 + 0.087 λ
Max, min transmission	0.9497, 0.8739	0.9703, 0.9444
Extinction Model	Lorentzian Type-I	Gaussian Mixed
Extinction parameter	3.6(2) × 10^{-5}	Type I: 5.7(4) × 10^{-6} Type II: 6.5(2) × 10^{-5}
d_{min}, Å	0.5	0.5
No. of reflns	1178	1650
No. of reflns ($I > 3\sigma(I)$)[a]	803	1644
No. of parameters refined	32	13
Refinement method	Full-matrix least-squares on F^2	
R indices $R_w(F^2)$[b], $R(F^2)$[c]	0.103, 0.115	0.133,0.122
Max, min difference peaks (fm/Å^3)	0.573, −0.429	1.58, −0.559
Goodness-of-fit	1.24	1.75

[a] Outliers with $|F_o^2/F_c^2| > 2$ and $|F_c^2/F_o^2| > 2$ were rejected. [b] $R_w(F^2) = \{\Sigma[w(F_o^2 - F_c^2)^2]/\Sigma[w(F_o^2)^2]\}^{1/2}$. [c] $R(F^2) = \Sigma|F_o^2\Sigma F_c^2|/\Sigma|F_o^2|$.

The Mn environment consists of an octahedral arrangement of Ga2 and Ge2 atoms at the 12*e* sites. These Ga/Ge atoms lie at the center of square pyramids with Mn at the apex and Ga1 atoms (and Ge1 atoms for the paramagnetic sample) at the base. The Ga1 atoms at the 12*d* site sit in a distorted tetrahedron

(61) Bacon, G. E.; Dunmur, I. W.; Smith, J. H.; Street, R. *Proc. R. Soc. London, Ser. A* **1957**, *241*, 223–38.
(62) Oxley, D. P.; Tebble, R. S.; Williams, K. C. *J. Appl. Phys.* **1963**, *34*, 1362–3.
(63) Hastings, J. M.; Elliott, N.; Corliss, L. M. *Phys. Rev.* **1959**, *115*, 13–17.
(64) Mori, N.; Mitsui, T. *J. Phys. Soc. Jpn.* **1968**, *25*, 82–8.
(65) Bie, H. Y.; Zelinska, O. Y.; Tkachuk, A. V.; Mar, A. *Chem. Mater.* **2007**, *19*, 4613–4620.
(66) Teske, D.; Drumheller, J. E. *J. Phys.: Condens. Matter* **1999**, *11*, 4935–4940.

Table 4. Select Bond Lengths (Å) of Paramagnetic $Y_4Mn_{0.95}Ga_{8.0}Ge_{4.0}$ and Ferromagnetic $Y_4Mn_{0.90}Ga_{11.0}Ge_{1.0}$ from Neutron Refinements

	paramagnetic	ferromagnetic
Y1−Ga1	3.0356(7)	3.0398(7)
Y1−Ga2/Ge2	3.0542(7)	3.0588(7)
Mn1−Ga2/Ge2	2.4830(13)	2.4891(15)
Ga1−Ga2/Ge2	2.8078(10)	2.8100(11)

composed of the Ga/Ge atoms at the 12*e* site. Environments are drawn in Figure 5. Alternatively, the Mn atoms lie in one in every two octahedral holes created by a three-dimensional corner-sharing octahedral network of Ga and Ge atoms. A slice of the cell showing a plane of the Ga/Ge framework is depicted in Figure 6. The rare earth atoms sit in larger voids surrounded by 12 nearest neighbors of Ga and Ge. There are no Mn−Mn or Y−Mn bonds.

3.3.2. Modulated Structure of the Parent Ternary Compound $Y_4Mn_{1-x}Ga_{12}$. In the Ge-free ternary phase, single crystal X-ray diffraction experiments on $Y_4Mn_{1-x}Ga_{12}$ revealed additional supercell reflections centered at a commensurate distance of 1/6*a**, 1/6*b**, and 1/6*c** around main reflections, as shown in the X-ray diffraction synthetic precession photograph in Figure 7b, and correspond to the ordering of Mn vacancies at the 2*a* site and distortions in the framework formed by the Ga atoms. The absence of cross term satellite reflections (reflections coming from the addition and subtraction of modulation vectors) suggested the presence of three twin domains with a single 6-fold modulation vector rather than a single domain with three individual *q*-vectors. The commensurate supercell was solved using a (3 + 1)-dimensional crystallographic approach in the superspace group $Im(0\beta\gamma)0$ with a modulation vector of 1/6*b**. Additionally, three twin laws were applied with corresponding matrices of [0 1 0 −1 0 0 0 0 1], [1 0 0 0 0 1 0 1 0], and [0 0 −1 0 1 0 1 0 0]. The refined fractions of these twin domains were 81.5(2)%, 9.9(2)%, and 4.6(1)%, respectively. The fraction of the main domain, [1 0 0 0 1 0 0 0 1], was 4.0(3)%. The total agreement factor for all the 32108 reflections (9848 main + 22 260 satellites) was 6.97%. The modulated single crystal X-ray refinement data are summarized in Table 5. Atomic coordinates are given in Table 6. Anisotropic thermal parameters can be found in the Supporting Information.

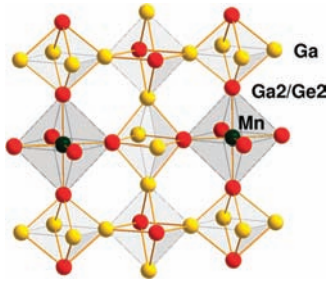

Figure 6. A slice of the unit cell depicting the corner-sharing octahedra formed by Ga (yellow) and Ga/Ge atoms (red). Mn atoms (green) sit in octahedra at the bcc positions of the cell. The Y atoms are omitted.

Table 5. Crystal Data and Structure Refinement for the Modulated Structure of $Y_4Mn_{0.74(1)}Ga_{12}$ at 100 K

Empirical formula	$Y_4Mn_{0.74(1)}Ga_{12}$
Formula weight	1232.8
Temperature	100.0(3) K
Wavelength	0.71073 Å
Crystal system	monoclinic
Space group	$Im(0\beta\gamma)0$
Unit cell dimensions	a = 8.5418(7) Å, α = 90° b = 8.5424(7) Å, β = 90° c = 8.5496(7) Å, λ = 90°
q-vector	1/6 b*
Volume	623.84(9) Å^3
Z	2
Density (calculated)	6.5608 g/cm^3
Absorption coefficient	44.444 mm^{-1}
F(000)	1093
Crystal size	0.20 × 0.14 × 0.10 mm^3
Theta range for data collection	3.1° to 35.9°
Index ranges	$-13 \le h \le 13$, $-13 \le k \le 13$, $-14 \le l \le 13$, $-1 \le m \le 1$
Reflections collected	15 980 (4861 main +11 119 satellites)
Independent reflections	6558 (2881 main +3677 satellites) [R_{int} = 0.0692]
Completeness to θ = 34.53°	98%
Refinement method	Full-matrix least-squares on F^2
Data/restraints/parameters	6558/0/179
Goodness-of-fit on F^2	1.95
Final R indices [$I > 3\sigma(I)$][a]	R_{obs} = 0.0675, wR_{obs} = 0.1670
R indices (all data)	R_{all} = 0.1358, wR_{all} = 0.1959
Final R main indices [$I > 3\sigma(I)$]	R_{obs} = 0.0582, wR_{obs} = 0.1462
R main indices (all data)	R_{all} = 0.0794, wR_{all} = 0.1581
Final R 1st order satellites [I > 3σ(I)]	R_{obs} = 0.1103, wR_{obs} = 0.2220
R 1st order satellites (all data)	R_{all} = 0.3166, wR_{all} = 0.2856
Extinction coefficient	60(30)
T_{min} and T_{max} coefficients	0.0096 and 0.0642
Largest diff. peak and hole	9.52 and −5.03 e·Å^{-3}

[a] $R = \Sigma||F_o| - |F_c||/\Sigma|F_o|$, $wR = \{\Sigma[w(|F_o|^2 - |F_c|^2)^2]/\Sigma[w(|F_o|^4)]\}^{1/2}$ and $w = 1/(\sigma^2(I) + 0.0016I^2)$.

The Mn deficiency is substantially greater in the ternary Ge-free phase than in the quaternary analogues with a preference for an ordered rather than random distribution of atoms and vacancies. The long-range ordering of vacancies at the Mn site and positional modulation on all atoms create a distribution of distances between Ga−Ga atoms with a minimum distance of 2.866(6) Å and maximum of 3.609(6) Å. The largest displacement was found for Ga8 (±0.3 Å), which is located above and

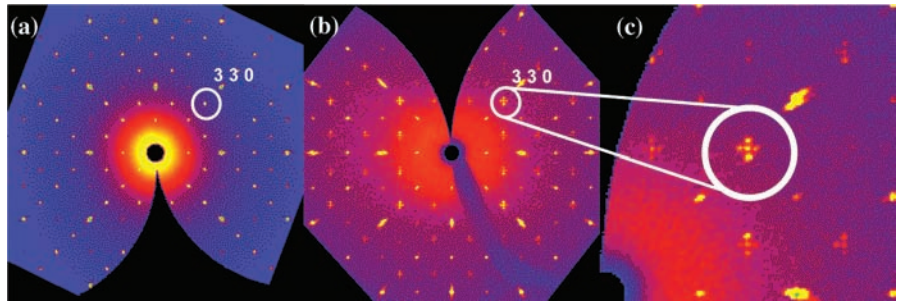

Figure 7. Synthetic precession photographs (*hk*0) generated from X-ray diffraction data for (a) quaternary $Y_4Mn_{1-x}Ga_{12-y}Ge_y$ and (b) ternary $Y_4Mn_{0.74}Ga_{12}$ viewed down [001]. (c) A zoomed-in image shows that satellite peaks (330 reflection circled) are clearly present in the ternary phase about *h*, *k*, 0 reflections that meet the condition $h, k = 2n + 1$. No satellite peaks are observed in the quaternary phase.

Table 6. Atomic Coordinates ($\times 10^4$), Fourier Components of the Displacive Modulation ($\times 10^4$) and Equivalent Isotropic Displacement Parameters ($Å^2 \times 10^4$) for $Y_4Mn_{0.74(1)}Ga_{12}$ at 100.0(3) K with Estimated Standard Deviations in Parentheses

Atom	Wave	*x*	*y*	*z*	Occupancy	U_{eq}
Y(1)	0	2500	2500	0	1	6(1)
	sin,1	0	0	0		
	cos,1	52(6)	0	54(6)		
Y(2)	0	2500	7500	0	1	5(1)
	sin,1	0	0	0		
	cos,1	−52(6)	0	−53(6)		
Ga(1)	0	0	0	0	1	8(1)
	sin,1	0	0	245(13)		
	cos,1	0	0	204(12)		
Ga(2)	0	2645(2)	0	7500	1	6(1)
	sin,1	238(3)	0	0		
	cos,1	0	50(6)	0		
Ga(3)	0	5000	0	5187(5)	1	5(1)
	sin,1	0	0	−257(8)		
	cos,1	0	0	0		
Ga(4)	0	0	2346(6)	7500	1	5(1)
	sin,1	0	472(11)	0		
	cos,1	0	243(16)	0		
Ga(5)	0	0	7500	7500	1	8(1)
	sin,1	0	−487(7)	0		
	cos,1	0	0	0		
Ga(6)	0	0	2540(5)	2500	1	5(1)
	sin,1	0	−193(9)	0		
	cos,1	0	0	0		
Ga(7)	0	0	7417(5)	2500	1	7(1)
	sin,1	0	191(9)	0		
	cos,1	0	0	0		
Ga(8)	0	2349(3)	0	2500	1	7(1)
	sin,1	402(4)	0	27(7)		
	cos,1	0	−88(7)	0		
Ga(9)	0	0	0	4866(4)	1	9(1)
	sin,1	0	0	−351(11)		
	cos,1	0	0	−165(15)		
Ga(10)	0	5000	0	9761(5)	1	6(1)
	sin,1	0	0	314(6)		
	cos,1	0	0	0		
Mn(1)	0	5000	0	2500	0.478(5)	3(1)
	sin,1	0	0	0		
	cos,1	0	100(7)	0		
Mn(2)	0	0	0	7500	0.260(6)	3(1)
	sin,1	0	−135(11)	0		
	cos,1	0	0	0		

below the Mn atoms along the *a*-axis (Ga/Ge position (red) in Figure 5). The displacive modulation wave along the *a*-direction for Ga8 is graphed in Figure 8. Mn atom sites are partially occupied at the octahedral position surrounded by Ga atoms as in the subcell, but their distribution with vacancies was found to be discontinuous, shown in Figure 8. Since the atomic domain along the fourth dimension was not continuous for the Mn atoms, a special step Crenel function was used, Figure 9, and centered on the electron density (solid blue lines in Figure 8). The refined occupancy on the Mn sites gave the final formula of $Y_4Mn_{0.74(1)}Ga_{12}$.

Mn-filled and empty Ga octahedra are separated in slabs that layer along the 6-fold *b*-axis. Figure 10 shows a two-dimensional plane of the modulated structure perpendicular to the *c*-axis through the center of the Ga octahedra ($z = 0$). Yttrium atoms lie above the plane at $z = 0.25$. The maximum bond length shown is 2.92 Å. Disturbance of the Ga−Ga bonding pattern is clearly visible at the border between Mn-filled and vacant regions. The minimum Mn−Ga distance is 2.316(3) Å, and the maximum 2.610(7) Å. The shortest Y−Ga distance is 2.957(5) Å, and the longest one 3.088(5) Å. The position of the Ga atoms next to the Mn atoms or vacancies modulates accordingly so

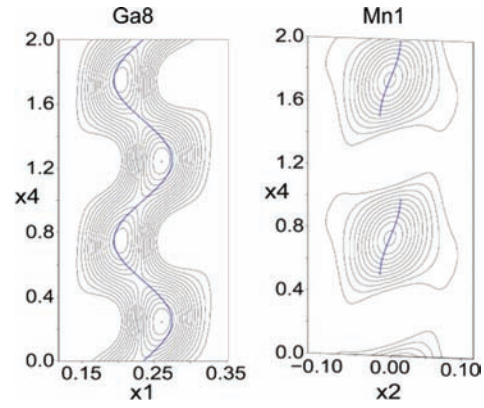

Figure 8. Contour plot of the Ga8 atom along the x1(*a*-axis)−x4(fourth dimension) direction (left) and Mn1 atom along the x2(*b*-axis)−x4(fourth dimension) direction (right). Each black solid line represents an electron density of 10 e•A^{-3}. The atomic domain of the refined structure is shown in solid blue line. Note that the electron density for Mn1 is not continuous along the fourth direction; the application of a Crenel function yielded the correct atomic domain shown in solid blue lines.

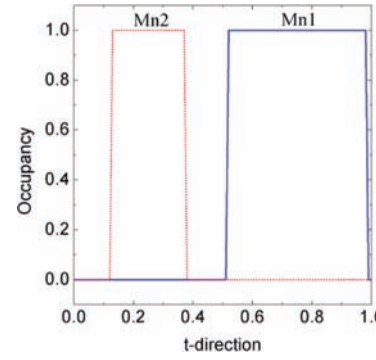

Figure 9. Step-like modulation of the occupancy of Mn1 and Mn2 atoms along the t-direction (position of subcell relative to supercell along the modulation direction) after the use of a Crenel function.

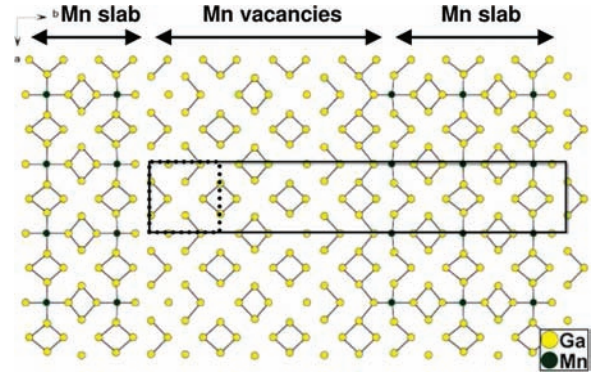

Figure 10. Two-dimensional view down the *c*-axis ($z = 0$) showing the modulation of Ga−Ga and Mn−Ga bond lengths in ternary $Y_4Mn_{0.74}Ga_{12}$. The subcell is outlined in dashes within the 6-fold commensurate cell. Bonds are drawn at less than 2.92 Å.

where there is no Mn in the octahedral site the Ga-octahedron shrinks. The unfilled octahedra are significantly contracted with respect to the average structure and show a compression and relaxation pattern along the *b*-direction.

Recently, the series RE_4FeGa_{12} (RE = Y, Tb, Dy, Ho, and Er) was reported.[45] The Y_4FeGa_{12} compound was analyzed for magnetic susceptibility and found to be a weak itinerant ferromagnet with a $T_c = 36$ K. In the Y analogue, as well as in

the Tb, Dy, and Ho analogues, Fe is fully occupied on the 2*a* site and Ga is stable on the 12*d* and 12*e* sites. Interestingly, it is the Er analogue, $Er_4Fe_{0.67}Ga_{12}$, in which Fe becomes deficient and the 12*e* Ga site splits between two positions that correspond to compressed Ga octahedra in the absence of Fe, although without long-range order as observed in $Y_4Mn_{0.74}Ga_{12}$. The creation of vacancies, as the authors suggest, seems to be induced by a decrease in RE size and, correspondingly, lattice parameter. With room temperature lattice parameters lying above those of Tb_4FeGa_{12} and $Er_4Fe_{0.67}Ga_{12}$, $a = 8.5610(4)$ and 8.4760(3), respectively, Fe is fully occupied in $TbFeGa_{12-x}Ge_x$ ($x = 2.5$) with $a = 8.5620(9)$ (XRD)[38] and consistent with this size effect concept. Here, addition of Ge does not affect Fe occupancy and the structure is stable with or without disorder. In the case of $Y_4Mn_{1-x}Ga_{12-y}Ge_y$, size effects based on lattice parameters can only explain the large difference in Mn occupancy between the quaternary and ternary phase. The opposite trend is observed between the ferromagnetic and paramagnetic quaternary phases. The stability of the Mn phases is most likely determined by a combination of Mn vacancies, Ge concentration, the magnitude of positional distortions, and perhaps also how evenly Ge distributes over the two 12*d* and 12*e* sites. From the neutron diffraction experiments, we find that Ge is nearly evenly distributed in the paramagnetic phase but, at $y = 1.0$, Ge is contained solely on the 12*e* site.

The separation of Mn atoms into discrete layers in $Y_4Mn_{0.74}Ga_{12}$ is in contrast to the quaternary paramagnetic phase in which the Mn sites are close to fully occupied. It is reasonable to suspect, however, that a similar separation of Mn atoms occurs to some degree at low Ge concentrations in the quaternary systems. Although additional satellite peaks were not observed owing to a lack of long-range order of Mn vacancies in the quaternary samples, the close proximity of the residual densities seen in the ferromagnetic X-ray data refinement may be evidence for a moderately modulated structure. These variations in local and long-range structure created by vacancies and disorder may be responsible for variation in magnetic properties, as is proposed for example in CaB_6.[67,68] Consistent with studies with Fe,[45] to stabilize Y, Mn, and Ga in the Y_4PdGa_{12} structure type Mn vacancies must be created. This deficiency results in modulation of bond lengths. To maintain full Mn occupation, Ge must be added to the system as an n-type substitution for Ga.

(67) Moriwaka, T.; Nishioka, T.; Sato, N. K. *J. Phys. Soc. Jpn.* **2001**, *70*, 341–344.
(68) Edwards, D. M.; Katsnelson, M. I. *J. Phys.: Condens. Matter* **2006**, *18*, 7209–7225.

4. Concluding Remarks

The $Y_4Mn_{1-x}Ga_{12-y}Ge_y$ system represents a unique series of compounds of the Y_4PdGa_{12} structure type in which a combination of Mn site vacancies and Ge atom concentration controls the magnetic interactions between the Mn atoms. An intimate relationship exists between Mn and the octahedral Ga and Ge atoms surrounding them. The Ge atom concentration can tune the Mn atom vacancy in the structure, which has a profound effect on the magnetic properties of the system. At the highest Ge fraction synthesized in this study, at $y = 4.0$, the compounds are paramagnetic. Ferromagnetism, with a relatively high T_c of nearly 230 K at the maximum, develops in a tunable fashion as Ge concentration gradually decreases. Mn vacancies also begin to develop as Ge decreases, and in the total absence of Ge, $y = 0$, Mn atoms and vacancies order into slabs of Mn-filled octahedra and Mn-free octahedra creating a 6-fold modulated structure and bond fluctuations that propagate throughout the crystal structure. To our knowledge the $Y_4Mn_{1-x}Ga_{12-y}Ge_y$ system is the first example where ferromagnetism can be induced by controlling the vacancies of the magnetic species. Electronic band structure calculations, using appropriate supercell models, are needed to help explain the driving force for the ordering and how the introduction of Ge in the structure affects the magnetic interactions.

Acknowledgment. Research supported by the U.S. Department of Energy, Office of Basic Energy Sciences, Division of Materials Sciences and Engineering under Award DE-FG02-07ER46356. The SEM EDS work was performed in the EPIC facility of NUANCE Center at Northwestern University. NUANCE Center is supported by NSF-NSEC, NSF-MRSEC, Keck Foundation, the State of Illinois, and Northwestern University. Trace metals analysis was performed in the IMSERC facility at Northwestern University and supported by the National Science Foundation. Work at Argonne National Laboratory was supported by the U.S. Department of Energy, Office of Science, Office of Basic Energy Sciences, under Contract DE-AC02-06CH11357. Experiments at the ISIS Pulsed Neutron and Muon Source were supported by a beam time allocation from the Science and Technology Facilities Council.

Supporting Information Available: Experimental powder X-ray diffraction patterns; tables of crystallographic data, refinements, and related information for $Y_4Mn_{1-x}Ga_{12-y}Ge_y$. This material is available free of charge via the Internet at http://pubs.acs.org.

JA1009986